Green Chemistry

RSC Publishing

COMMUNICATION

View Article Online
View Journal | View Issue

Cite this: *Green Chem.*, 2013, **15**, 3015

Received 7th June 2013,
Accepted 12th August 2013

DOI: 10.1039/c3gc41089g

www.rsc.org/greenchem

Ammoxidation of allyl alcohol – a sustainable route to acrylonitrile†

Cyrille Guillon,[a,b] Carsten Liebig,[a,b,c] Sébastien Paul,[b,d] Anne-Sophie Mamede,[a,b] Wolfgang F. Hölderich,[c] Franck Dumeignil[a,b,e] and Benjamin Katryniok*[b,d]

The ammoxidation of allyl alcohol was demonstrated over antimony–iron oxide catalysts with a Sb/Fe ratio of 0.6 and 1. Both catalysts showed high performance with 83 and 84% yield of acrylonitrile, respectively, whereby the main difference was found in the initial performance. This was ascribed to the *in-operando* formation of the $SbFeO_4$ mixed oxide on the catalyst surface under reaction conditions, as proven by XPS analysis.

Acrylonitrile is an important building block in the chemical industry with a major application in polymers such as acrylic fibers, ABS (acrylonitrile-butadiene-styrene) and SAN (styrene-acrylonitrile). Thus, it can be found in several daily life products such as hard-sided luggage or LEGO® bricks or – after carbonization of the acrylic fibers – as carbon fiber for high performance applications like in aviation.[1] Besides this direct application as a monomer, acrylonitrile is also used as an intermediate for the production of adiponitrile and acrylamide.[2]

Nowadays, acrylonitrile is exclusively obtained from fossil sources, namely *via* the ammoxidation of propylene in the presence of ammonia and air. This technology is also known as the SOHIO process, which is based on a complex multi-component catalyst and – due to the exothermicity of the reaction – carried out in a fluidized bed to enable a yield of *ca.* 80% of acrylonitrile.[3–5] Since the development of the corresponding process by Standard Oil of Ohio in the 1960s, the interest in other starting materials for producing acrylonitrile has rather focused on alkanes – namely propane[6–8] – which is not a sustainable resource. Hence, a renewable substrate for the synthesis of acrylonitrile was desirable. With respect to the three carbon backbone of acrylonitrile, glycerol was reported as a potential starting material. Thus, two processes are described in the literature, namely a direct synthesis in gas or liquid phase – employing microwave heating in the latter case,[9,10] as well as an indirect synthesis *via* acrolein as an intermediate. We recently reported on the last mentioned two-step conversion of glycerol to acrylonitrile, involving first a dehydration step followed by an ammoxidation step.[11] Whereas the gas phase dehydration of glycerol is well-known to be catalysed by various solid acid catalysts (*i.e.* zeolites, niobia and supported inorganic acids) enabling high yields of up to 95%,[12–14] the ammoxidation of acrolein – notably in a vapor rich atmosphere – is only poorly studied.[15,16] Thus, the latter was identified as the limiting step of this two-step process. In fact, the ammoxidation of acrolein over the antimony–iron mixed oxide catalyst did not surpass 40% yield of acrylonitrile. This limitation encouraged us to rethink the process, which is commonly based on acrolein as a reaction intermediate due to the historical use of propylene as a starting material. Inspired by the fact that allyl alcohol is a well known probe molecule when studying the mechanism involving allyl intermediates,[17] we herein report the ammoxidation of allyl alcohol to acrylonitrile. Nowadays, allyl alcohol is conventionally obtained from acrolein by selective hydrogenation or from propylene oxide.[18] Nevertheless, it can also be obtained from renewable sources such as glycerol[19,20] or 1,2-propane-diol.[21] Thus, the ammoxidation of allyl alcohol (Scheme 1) is a promising way for a sustainable synthesis of acrylonitrile. In fact, the only previous report available is a patent of Distillers Company from 1950 using an iron-molybdate catalyst and yielding barely 40% acrylonitrile but together with 34% carbon dioxide.[22] Here, we report the use of

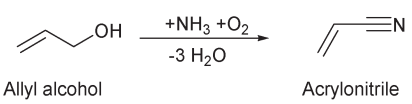

Scheme 1 Ammoxidation of allyl alcohol to acrylonitrile.

[a]*Univ. Lille Nord de France, F-59000 Lille, France*
[b]*Unité de Catalyse et de Chimie du Solide, UCCS (UMR CNRS 8181), Cité Scientifique, F-59650 Villeneuve d'Ascq, France.*
E-mail: benjamin.katryniok@ec-lille.fr
[c]*Department of Chemical Technology and Heterogeneous Catalysis, RWTH Aachen University, Worringerweg 1, D-52074 Aachen, Germany*
[d]*Ecole Centrale de Lille, ECLille, F-59655 Villeneuve d'Ascq, France*
[e]*Institut Universitaire de France, Maison des Universités, 103 Boulevard Saint-Michel, 75005 Paris, France*

†Electronic supplementary information (ESI) available: Experimental, information about the design of experiment approach and reproducibility. See DOI: 10.1039/c3gc41089g

Table 1 Analysis results for antimony–iron catalysts

	EDX analysis		N_2 physisorption		
Sb/Fe theor.	Elemental composition (O/Fe/Sb)[a]	Sb/Fe[a]	S_{BET} ($m^2\ g^{-1}$)	V_{pore} ($cm^3\ g^{-1}$)	XPS Sb/Fe[a]
0.6	0.48/0.32/0.20	0.63	24.0	0.080	0.58 (1.63)
1.0	0.44/0.30/0.26 (0.45/0.29/0.26)	0.87(0.89)	11.3	0.034	1.43 (1.54)

theor. = theoretical ratio; exp. = experimental ratio; S_{BET} = specific surface area; V_{pore} = pore volume. [a] Value for spent catalyst in brackets.

an antimony–iron oxide catalyst yielding up to 83% acrylonitrile under optimized reaction conditions.

Two antimony–iron oxide catalysts were prepared with a Sb/Fe ratio of 0.6 and 1, respectively. The detailed procedure and all experimental details are presented in the ESI.† The catalysts were analyzed by different techniques to determine the bulk and surface compositions as well as the surface texture. The determination of the bulk composition was performed by X-ray diffraction and EDX analysis. The elemental composition determined by EDX roughly confirmed the theoretical ratio used for the synthesis of the catalysts (Table 1). In fact, for the catalyst with a theoretical Sb/Fe ratio of 1, we observed an experimental value of 0.87, whereas the catalyst with a theoretical ratio of 0.6 exhibited an experimental Sb/Fe ratio of 0.63. With respect to a possible leaching of metals due to the large amount of water vapor under the reaction conditions (85%), the elemental composition of the Sb/Fe catalyst with a ratio of 1 was determined after the test. From the results (Table 1), one can clearly see that the elemental composition after the test remained unchanged (Sb/Fe 0.89 *vs.* 0.87 initially), supporting thus the stability of the catalyst under the reaction conditions.

From the XRD results (Fig. 1), one can see that the catalyst with an antimony/iron ratio of 0.6 exhibited two main phases, namely iron-III-oxide (JCPDS 33-0664) and antimony-III-oxide (JCPDS 43-1071). Furthermore, smaller amounts of

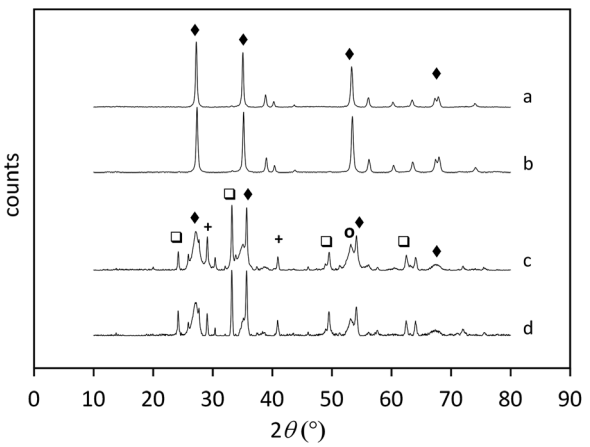

Fig. 1 XRD diffractograms for catalysts with Sb/Fe = 1.0 fresh (b) and after the test (a); Sb/Fe = 0.6 fresh (d) and after the test (c), showing Sb_2O_3 (○), Fe_2O_3 (□), $SbFeO_4$ (◆) and SbO (+).

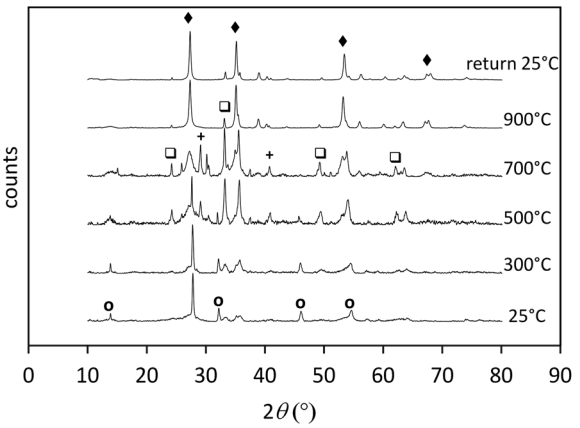

Fig. 2 Temperature-programmed XRD diffractograms for catalysts with Sb/Fe = 1.0, showing Sb_2O_3 (○), Fe_2O_3 (□), $SbFeO_4$ (◆) and Sb_2O_4 (+).

antimony-III–V-mixed oxide (JCPDS 11-0694) and antimony–iron-mixed oxide (JCPDS 34-0372) can be observed. Comparable results were also observed for the catalyst with a Sb/Fe ratio of 1 when the latter was calcined at a low temperature of 500 °C (Fig. 2). On the other hand, the calcination at 900 °C yielded quantitative formation of the iron–antimony mixed oxide (*cf.* Fig. 1b and 2). Comparable results were also reported by Allen *et al.*[23] It is also worth mentioning that both catalysts exhibited identical XRD patterns after the reaction (Fig. 1a and 1c).

Concerning the textural properties (Table 1), both catalysts exhibited rather low specific surface areas of 24 $m^2\ g^{-1}$ (Sb/Fe = 0.6) and 11.3 $m^2\ g^{-1}$ (Sb/Fe = 1). The significantly lower value for the catalyst with the Sb/Fe ratio of 1 was ascribed to the higher calcination temperature (900 °C *vs.* 500 °C), which strongly promoted the sintering of the crystallites, whereby the pore volume – and thus the specific surface area – decreased inevitably.

In order to determine the surface composition and oxidation states of the surface species, both catalysts were also analysed by X-ray photoelectron spectroscopy. C 1s, Fe 2p, O 1s and Sb 3d photopeaks and the Sb $M_4N_{4,5}N_{4,5}$ Auger line were recorded. It has to be noted that the most intense photopeaks of O 1s and Sb $3d_{5/2}$ are overlapped, so the Sb $3d_{3/2}$ peak was used. Thus, based on the Sb $M_4N_{4,5}N_{4,5}$ Auger line, XPS data are presented as a Wagner plot (Fig. 3) to determine the Sb chemical environment.

In both catalysts, antimony and iron are present as Sb(V) and Fe(III) in an oxide environment, respectively. Indeed, their Sb $3d_{3/2}$ binding energy (BE) values are higher (540.8 eV for Sb/Fe = 1 and 540.5 eV for Sb/Fe = 0.6) than the BE value of the reference oxide, Sb_2O_5 (540.4 eV). Likewise, a positive shift for Fe $2p_{3/2}$ BE is observed between the reference Fe_2O_3 (710.8 eV)[24] and both catalysts (711.8 eV for Sb/Fe = 1 and 711.2 eV for Sb/Fe = 0.6). Consequently, these significant BE shifts seem to be characteristic of the presence of mixed oxide on the surface of the catalyst. Unfortunately, it was not possible to differentiate between oxides (Fe_2O_3, Sb_2O_3 and Sb_2O_4) and $FeSbO_4$ mixed oxide, as detected by DRX.

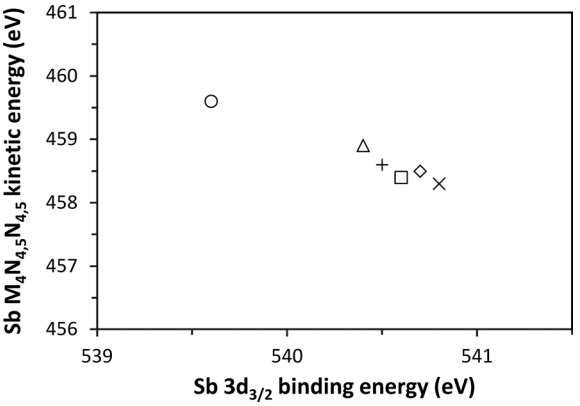

Fig. 3 Results of XPS analysis presented as a Wagner plot: (x) catalyst Fe/Sb = 1 fresh, (◊) catalyst Fe/Sb = 1 after the test, (+) catalyst Fe/Sb = 0.6 fresh, (□) catalyst Fe/Sb = 0.6, (△) Sb_2O_5 and (○) Sb_2O_3.

Furthermore, we determined the antimony/iron ratio at the surface of the catalyst (XPS analysis depth less than 10 nm). The results (Table 1) show that the corresponding ratio is very close to the theoretical value for the catalyst with a Sb/Fe ratio of 0.6 (0.58), which also indirectly confirms the homogeneity of the sample, as the bulk ratio determined by EDX exhibited the same value. On the other hand, the catalyst with a theoretical ratio of 1 exhibited significant enrichment in antimony at the surface (a Sb/Fe ratio of 1.48). This is notably in contrast to the bulk ratio, which was determined at 0.87, suggesting thus a migration of Sb from the bulk to the surface.

The outermost atomic layer of both catalysts was also analysed by LEIS (Fig. 4). They exhibit different elemental compositions. Indeed, the catalyst with Sb/Fe = 1 presents a Sb/Fe ratio of 1.4, which confirms the XPS results and illustrates that the outermost atomic layer is identical to the 10 nm surface layer. Likewise, the catalyst with Sb/Fe = 0.6 presents a Sb/Fe ratio of 0.8, which is also close to the XPS results (Sb/Fe = 0.58) and confirms the homogeneous composition of the surface.

Finally, both catalysts were also analysed by XPS after the test. Whereas the catalyst with a theoretical Sb/Fe ratio of 1 remained rather unchanged with a Sb/Fe surface ratio of 1.54 (*vs.* 1.43 initially), the catalyst with the theoretical ratio of 0.6 showed significant changes. In fact, the latter showed significant enrichment in antimony at the surface after the test (ratio of 1.63 *vs.* 0.58 initially). This increase was ascribed to the formation of the $FeSbO_4$ mixed phase under the reaction conditions, as after the test, both catalysts exhibit nearly identical elemental composition and chemistry, as can be seen in Fig. 3. Nevertheless, as no change was detected by XRD (*cf.* Fig. 1), the modification remains limited to the surface of the catalyst. The formation of the mixed phase most probably took place during the very first hour of reaction, which is accompanied by an increase in selectivity to acrylonitrile (*vide infra*).

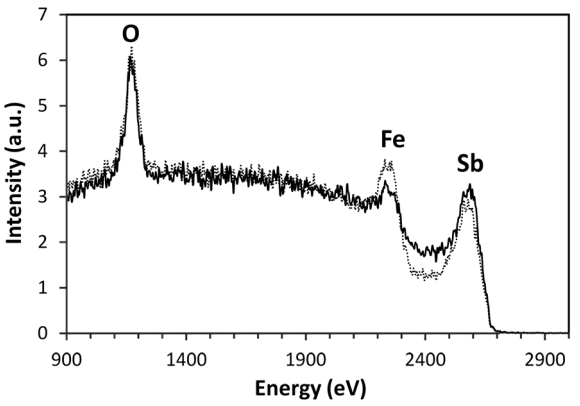

Fig. 4 LEIS spectra (3 keV $^4He^+$) of catalysts with Sb/Fe = 1 (straight line) and Sb/Fe = 0.6 (dotted line).

Table 2 Catalytic performances in the ammoxidation of allyl alcohol

	Before DoE[a]		After DoE[b]	
Sb/Fe ratio	1	0.6	1	0.6
C (%)	99	100	100	100
S_{ACN} (%)	59	67	84	83
S_{AC} (%)	8	11	3	4
S_{AN} (%)	4	4	3	3
CB (%)	80	97	91	92

[a] 400 °C; AllylOH/O_2/NH_3 ratio 1/3.5/2; contact time 0.1 s; 4 h reaction time. [b] 450 °C; AllylOH/O_2/NH_3 ratio 1/3.5/3; contact time 0.16 s; 4 h reaction time; DoE = design of experiment; C = conversion; S_{ACN} = selectivity to acrylonitrile; S_{AC} = selectivity to acrolein; S_{AN} = selectivity to acetonitrile; CB = carbon balance.

In the first stage of the work, both catalysts were tested under reaction conditions inspired by Liebig *et al.* (400 °C; AllylOH/O_2/NH_3 ratio 1/3.5/2; contact time 0.1 s).[11] From the results (Table 2), one can see that both catalysts exhibited full conversion at 400 °C. On the other hand, the selectivity to acrylonitrile was 59% and 67% over the catalyst with a Sb/Fe ratio of 1.0 and 0.6, respectively. The other products observed were acrolein (a selectivity of 8% and 11%, respectively, over the catalyst with a Sb/Fe ratio of 1.0 and 0.6), acetonitrile (4%), acetaldehyde and propionaldehyde (the latter two with a selectivity of <3%). In the following, the influence of the different reaction parameters (reaction temperature, allyl alcohol/ammonia ratio and contact time) was studied. In order to take into account cross-interactions between the reaction parameters as well as to reduce the number of necessary experiments, we adopted a computer assisted experimental design (explanation and results of the individual experiments are reported in the ESI†). The corresponding predictions are shown in Fig. 5 and 6. Thus one can see that the yield of acrylonitrile is predicted to significantly increase with the reaction temperature. In fact, the yield increased from less than 10% to over 80% when the temperature was increased from 350 °C to 450 °C. Concerning the impact of the ammonia/allyl alcohol ratio, a strong increase in yield (*i.e.*, from 45% to 75% for 450 °C) is predicted when increasing the latter from 1.0 to 2.0. On the other hand, a further increase to 3.0 shows only a slight amelioration in yield (*i.e.* from 75% to 85% for 450 °C). Finally, the influence of the contact time (by using different amounts of catalyst) was studied. Surprisingly, the model

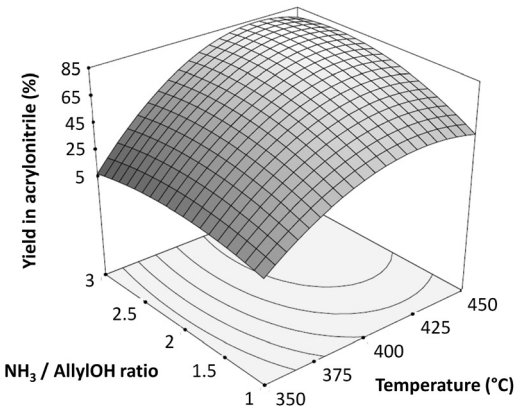

Fig. 5 Yield of acrylonitrile as a function of reaction temperature and ammonia/allyl alcohol ratio (contact time = 0.16 s) as predicted by the model of the experimental design approach.

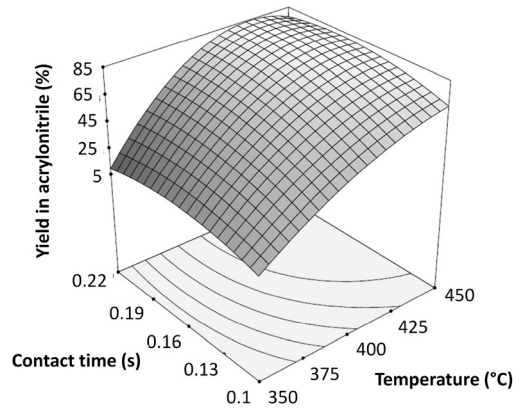

Fig. 6 Yield of acrylonitrile as a function of reaction temperature and contact time (NH_3/AllylOH ratio = 2.7) as predicted by the model of the experimental design approach.

predicts that the impact of the contact time is rather low compared to the other mentioned parameters. In fact, when increasing the contact time from 0.1 s to 0.16 s, the yield increases from 65% to 80–85% (reported for 450 °C reaction temperature). On the other hand, a further increase of the contact time to 0.2 s is foreseen to have nearly no more an impact on the yield of acrylonitrile. Thus, in the following, the catalysts were tested under the predicted optimized reaction conditions, namely 450 °C, an AllylOH/NH_3 ratio of 3 and a contact time of 0.16 s. From the results (Table 2), one can see that the experimental yield indeed corresponded to the predicted yields (80–85%), as both catalysts (a Sb/Fe ratio of 0.6 and 1.0) exhibit nearly identical yield of 83% and 84%, respectively. Compared to the results obtained before the parameter optimisation, this increase in acrylonitrile yield is accompanied by a decrease in the acrolein yield (3–4% *vs.* 8–11% initially). On the other hand, the yield of acetonitrile was rather constant (3% *vs.* 4% initially), which clearly shows that even at increased reaction temperature, the C–C bond cleavage was limited.

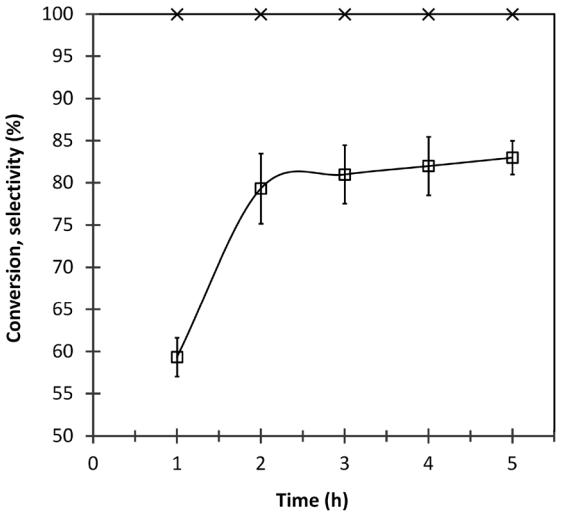

Fig. 7 Mean values for conversion (x) and selectivity to acrylonitrile (□) over the catalyst with Sb/Fe = 0.6 as a function of reaction time (450 °C, AllylOH/O_2/NH_3 ratio 1/3.5/3; contact time 0.16 s); error bars correspond to twice the standard deviation.†

Concerning the catalytic performance with time on stream, one can observe an increase in selectivity to acrylonitrile during the first hour of reaction in the case of the antimony–iron catalyst with a Sb/Fe ratio of 0.6 (Fig. 7), a result which was not observed over the catalyst with a ratio of 1 (not shown). This behaviour was ascribed to the formation of the $SbFeO_4$ mixed phase under the reaction conditions, which is in agreement with the characterisation of the spent catalyst (*vide supra*) and also confirms previous results obtained for the ammoxidation of acrolein.[11]

Conclusion

The ammoxidation of allyl alcohol provides a viable pathway for obtaining acrylonitrile. Compared to previously reported results for the ammoxidation of acrolein, the yield of acrylonitrile from allyl alcohol is significantly higher (84% *vs.* 36%) and the formation of by-products is significantly decreased, which is a clear advantage with regard to the principles of green chemistry. Furthermore, the $FeSbO_4$ mixed oxide was identified as the active phase. In the case of the non-stoichiometric catalyst, the latter was formed *in operando* during the first hour of the reaction, as proven by XPS analysis. This formation was also accompanied by an increase in selectivity to acrylonitrile.

Acknowledgements

The authors thank the Centrale Initiatives Foundation and the European Framework Programme FP7 (grant no. 241718) for financial support. Furthermore, we kindly thank Mr A. Beaurain for the XPS analysis.

Notes and references

1 M. K. Jain and A. S. Abhiraman, *J. Mater. Sci.*, 1987, **22**, 278.
2 J. F. Bradzil, *Kirk-Othmer Encyclopedia of Chemical Technology*, Wiley & Sons, 2010.
3 J. J. F. Brazdil Jr., D. Suresh Dev and R. K. Grasselli, US4746753, 1988.
4 R. Nilsson, T. Lindblad and A. Andersson, *Catal. Lett.*, 1994, 409.
5 Y. Takachika, S. Shigeru, S. Yutaka and N. Isao, US3542843, 1970.
6 T. Shishido, T. Konishi, I. Matsuura, Y. Wang, K. Takaki and K. Takehira, *Catal. Today*, 2001, **71**, 77.
7 M. Cimini, J. M. M. Millet, N. Ballarini, F. Cavani, C. Ciardelli and C. Ferrari, *Catal. Today*, 2004, **91–92**, 259.
8 C. Paparizos, M. J. Seely, J. F. JR. Brazdil and B. C. Sutradhar, WO2009048553, 2009.
9 M. O. Guerrero-Pérez and M. A. Banares, *ChemSusChem*, 2008, **1**, 511.
10 V. Calvino-Casilda, M. O. Guerrero-Perez and M. A. Banares, *Green Chem.*, 2009, **11**, 939.
11 C. Liebig, S. Paul, B. Katryniok, C. Guillon, J.-L. Couturier, J-L. Dubois, F. Dumeignil and W. Hölderich, *Appl. Catal., B*, 2013, **132–133**, 170.
12 B. Katryniok, S. Paul, V. Bellière-Bace, P. Rey and F. Dumeignil, *Green Chem.*, 2010, **12**, 2079.
13 A. Martin, U. Armbruster and H. Atia, *Eur. J. Lipid. Sci. Technol.*, 2012, **114**, 10.
14 B. Katryniok, S. Paul and F. Dumeignil, *ACS Catal.*, 2013, **3**, 1819.
15 H. Oka, K. Miyake, Y. Harano and T. Imoto, *J. Appl. Chem. Biotechnol.*, 1975, **25**, 663.
16 C. Eygen, P. Lambert and A. Hendrickx, GB1019372, 1962.
17 J. D. Burrington, C. T. Kartisek and R. K. Grasselli, *J. Catal.*, 1980, **63**, 235.
18 L. Krähling, J. Krey, G. Jakobson, J. Grolig and L. Miksche, *Ullmann's Encyclopedia of industrial chemistry*, Wiley-VCH, Weinheim, 2012.
19 E. Arceo, P. Marsden, R. G. Bergman and J. A. Ellman, *Chem. Commun.*, 2009, 3357.
20 W. Bühler, E. Dinjus, A. J. Ederer, A. Kruse and C. Mas, *J. Supercrit. Fluids*, 2002, **22**, 37.
21 S. Sato, R. Takahashi, T. Sodesawa, N. Honda and H. Shimizu, *Catal. Commun.*, 2003, **4**, 77.
22 F. J. Bellringer, T. Bewley and H. M. Stanley, GB709337, 1950.
23 M. D. Allen, S. Poulston, E. G. Bithell, M. J. Goringe and M. Bowker, *J. Catal.*, 1996, **163**, 204.
24 M. C. Biesinger, B. P. Payne, A. P. Grosvenor, L. W. M. Lau, A. R. Gerson and R. S. C. Smart, *Appl. Surf. Sci.*, 2011, **257**, 2717.